Chapter 4
Heat-Resistant Steel

Abstract The microstructure evolution of 10Cr ferritic/martensitic heat-resistant steel during creep at 600 °C is a main topic in this chapter. The 10Cr steel has higher creep strength than conventional ASME-P92 steel. The martensitic laths coarsen with time and eventually develop into subgrains during creep. Laves phase grows and clusters along the prior austenite grain boundaries during creep and causes the fluctuation of solution and precipitation strengthening effects. The microstructure evolution could be accelerated by stress. Laves phase is one of the most significant precipitates in ferritic/martensitic heat-resistant steels. Cobalt in the steel could accelerate the growth of Laves phase and coalescence of the large Laves phase would lead to the brittle intergranular fracture. Another topic of this chapter is the microstructural evolution during short-term thermal exposure of 9/12Cr heat-resistant steels, as well as mechanical properties after exposure. The tempered martensitic lath structure, as well as the precipitation of carbide and MX-type carbonitrides in the steel matrix is stable after 3,000 h exposure at 600 °C. During short-term thermal exposure process, the change of mechanical properties is mainly caused by the formation and growth of Laves phase precipitates.

4.1 Microstructure Before Creep and Creep Rupture Strength

After heat treatment, both the 10Cr steel and the P92 steel (Table 4.1) have tempered-martensite microstructures, with similar prior austenite sizes of about 20 μm. Prior austenite grain boundaries and lath boundaries are decorated by precipitates, $M_{23}C_6$ or MX, after tempering.

Figure 4.1 shows the relationship between the creep rupture strength and the rupture life at 600 °C in logarithmic plots for the two steels. The creep rupture strength generally decreases with the rupture life. However, the creep rupture strength of the 10Cr steel is higher than that of the P92 steel in the entire testing range. Under the creep rupture strength of 210 MPa, the rupture life of the 10Cr steel can reach about 8,354 h, which is much longer than that of the P92 steel, about 431 h. Therefore, the creep rupture strength of ASME-P92 could be improved by revising the chemical composition, like proper increase of the contents of chromium and tungsten as well as addition of cobalt.

W. Sha, *Steels*, DOI: 10.1007/978-1-4471-4872-2_4,

Table 4.1 Chemical compositions of heat-resistant steels (wt%)

Steels	C	Si	Mn	Cr	Mo	W	Co	Cu	Ni	V	Nb	N
P92	0.11	0.37	0.46	8.77	0.42	1.73	–	0.15	0.41	0.17	0.057	0.048
9Cr	0.09	0.31	0.50	8.58	0.40	1.65	1.64	–	0.39	0.18	0.060	0.040
10Cr	0.088	0.31	0.50	10.42	0.40	2.55	2.19	–	0.33	0.18	0.056	0.058

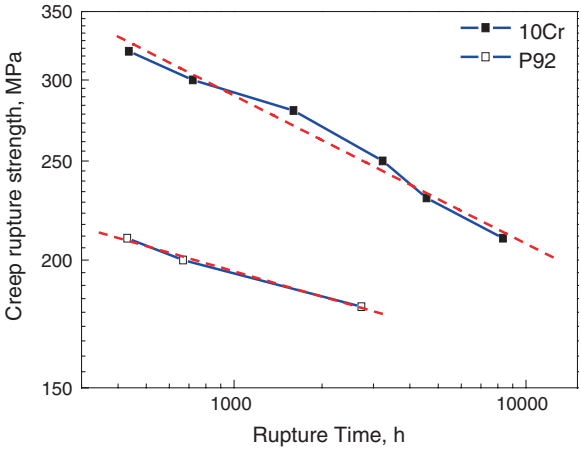

Fig. 4.1 Creep rupture strength versus rupture time of the steels at 600 °C. Reprinted from Hu et al. (2011) with permission from Elsevier

Moreover, two slope changes are seen from the curve of the creep rupture strength versus rupture time of the 10Cr steel. The slope of the curve first decreases after about 723 h and then increases after about 1,599 h. Since strength is dependent on microstructure, the two slope changes should be related to the microstructure evolution during creep.

4.2 Effect of Microstructure Evolution on Creep Rupture Strength

4.2.1 Martensitic Lath Structure

After normalising and tempering, the 10Cr steel acquires a tempered martensitic lath structure strengthened by $M_{23}C_6$-type carbides and MX-type carbonitrides. Most $M_{23}C_6$-type carbides are rod-shaped particles, 30–60 nm in width and 60–300 nm in length, mainly precipitated along lath boundaries. Most MX-type carbonitrides are spherical particles, 20 nm in size, and usually formed at dislocation sites inside the lath matrix. The high density of these fine precipitates could prevent the dislocation movement and the migration of the lath boundaries, resulting in a decrease in the creep rate. Therefore, they are desirable in the initial microstructure in order to improve the microstructure stability.

The mean width of the martensite laths increases with increase of the rupture life. The widened laths are further expanded and they finally evolve into subgrains after 8,354 h. Both lath widening and formation of subgrains during creep could be attributed to the continuous movement and annihilation of dislocations in the matrix and at the lath boundaries. The behaviour of dislocations follows a thermodynamic spontaneous process, since they are driven by the free energy difference between the martensite phase and the thermodynamically stable ferrite phase. Accompanied with lath widening and formation of subgrains usually is the decrease of both lath boundary area and dislocations density inside laths, which should be one of the main reasons for the slight decrease of creep rupture strength in Fig. 4.1.

4.2.2 Laves Phase

Creep deformation at elevated temperature should result from the migration of dislocations and subgrain boundaries (Maruyama et al. 2001; Hald 2008). Homogeneous distribution of fine and thermally stable precipitates can effectively pin the movement of dislocations and retard the coarsening of subgrains, resulting in the reduced creep rate. For the 9–12 wt% chromium ferritic/martensitic heat-resistant steels, there are mainly three types of precipitates. Both MX particles, where M could be Nb, V and Ti, and X could be C or N and $M_{23}C_6$, where M could be Cr, will precipitate after tempering treatment while $(Fe,Cr)_2(W,Mo)$, namely Laves phase, with a hexagonal crystal structure, can form during the long time creep. Research on these precipitates has shown that MX is the most stable and $M_{23}C_6$ is the second most stable precipitates. Both of them are small and very useful to the long-term stability of microstructure. However, Laves phase was observed to have the largest size and the highest coarsening rate. Therefore, the Laves phase is receiving more and more attention as a crucial component of the microstructure. The consumption of tungsten and molybdenum atoms in forming Laves phase will bring about counteraction between the solid solution strengthening and precipitation strengthening. Much work has been conducted to study the effect of Laves phase in this case. Lee et al. (2006) suggested that the precipitation strengthening due to the Laves phase could compensate the loss of solid solution strengthening in the early stage but the coarse Laves phase failed to compensate that loss in the later stage. Abe et al. (2007) seemed to find the similar result that the precipitation of Laves phase could reduce the creep rate but large coarsening of Laves phase promoted the creep rate at the acceleration creep stage after reaching a minimum creep rate in 9Cr-WVTa steels at 650 °C. However, they also found that large coarsening of Laves phase did not take place within their testing range at 600 °C so the precipitation of Laves phase could reduce the minimum creep rate and the steels had a longer rupture life, which was different from the opinion held by Lee et al. (2006). The work of Hald (2008) has revealed that size of the Laves phase remained steady, nearly 0.1 μm, after about 10,000 h creep

exposure; therefore, he suggested that precipitation strengthening of the Laves phase had more benefit to the microstructure stability and creep strength than the solid solution strengthening by tungsten and molybdenum atoms in P92 steel crept at 600 °C. This may explain the above beneficial effect of Laves phase on minimum creep at 600 °C found by Abe et al. (2007). All the research shows that the size of Laves phase is of great significance to the creep properties. Therefore, it is very important to carefully investigate the growth and coarsening behaviour of Laves phase in heat resisting steel.

In steel with high cobalt contents, the mean size of Laves phase was found to grow to 0.2 μm in a relatively short period of time of 1,598 h at 600 °C. Although Laves phase with the average size beyond 0.13 μm was discovered to trigger a fracture mode transition from ductile transgranular to brittle intergranular in the work of Lee et al. (2006) on P92 steel, brittle intergranular fracture did not always appear, in other steels. Therefore, the precipitation behaviour of Laves phase as well as its effect on the creep behaviour could be complex and will be investigated in Sects. 4.3–4.5 by considering the effect of cobalt on the nucleation and growth of Laves phase.

Microstructural examination of the 10Cr steel in the deformed section of the creep specimens suggests that Laves phase does not form after tempering (Hu et al. 2011). The evolution of Laves phase in the steel during creep shows that both the volume fraction and the mean size of Laves phase increase with the rupture life.

Tungsten, molybdenum, chromium and carbon all have homogeneous distribution in the 10Cr steel after tempering, whereas, after creep for 8,354 h, accumulation of tungsten, molybdenum, and chromium takes place in some regions. These tungsten-rich or molybdenum-rich regions are related to the formation of Laves phase. The chromium-rich or carbon-rich regions seem to be near or surrounding the tungsten-rich or molybdenum-rich regions. The granular or film-like Laves phase is formed adhering to the massive $M_{23}C_6$ along grain boundaries. Therefore, these chromium-rich or carbon-rich regions should be related to the $M_{23}C_6$-type carbides.

The Laves phase both inside the grains and along the prior austenite grain boundaries has larger size than the $M_{23}C_6$-type carbide, after creep for 8,354 h. Since Laves phase forms long after the $M_{23}C_6$-type carbide in the steel, it is implied that Laves phase must grow faster than $M_{23}C_6$-type carbide. After creep for 8,354 h, the mean size of Laves phase reaches about 0.3 μm.

Apart from the volume fraction and mean size, Laves phase also tends to cluster along the prior austenite grain boundaries. This clustering behaviour of Laves phase would greatly reduce the effect of Laves phase preventing the migration of the lath boundaries, and hence accelerate the lath widening and its evolution to subgrains.

In addition to the precipitation strengthening by $M_{23}C_6$-type carbides and MX-type carbonitrides, the solution strengthening from both tungsten and molybdenum atoms is an important strengthening mechanism for 9–12 %Cr ferritic/martensitic heat-resistant steels. However, formation of Laves phase is inevitable for this type of steels (Hasegawa et al. 2001). Since tungsten and molybdenum are the main elements of forming Laves phase, Fe_2W and Fe_2Mo, the formation of Laves phase would inevitably consume the dissolved tungsten and molybdenum atoms in the matrix and weaken solution strengthening.

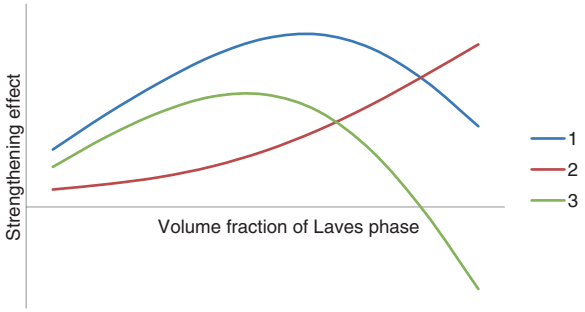

Fig. 4.2 Sketch diagram demonstrating the relationship between creep rupture strength and volume fraction of Laves phase. Curve 1: increase in creep rupture strength for precipitation strengthening effect caused by formation of Laves phase; curve 2: decrease in creep rupture strength for loss in solution strengthening caused by reduction in amount of solute atoms tungsten and molybdenum; curve 3: combined effect of curves 1 and 2

The two slope changes occurring on the creep rupture strength versus rupture time curve of the 10Cr steel as observed in Fig. 4.1 can also be well explained from the view of the precipitation behaviour of Laves phase. A sketch diagram qualitatively illustrating the relationship between the volume fractions of Laves phase and strengthening effect is presented in Fig. 4.2.

As mentioned above, on the one hand, formation of Laves phase consumes the solute atoms, tungsten and molybdenum, in the steel matrix, so the loss in solution strengthening from tungsten and molybdenum should be increased along with the increase of the volume fraction of Laves phase, as depicted by curve 2.

However, on the other hand, precipitation strengthening from Laves phase is not a monotonic increasing function of the volume fraction of Laves phase. It is affected by both the volume fraction and the mean size of Laves phase. The relationship between precipitation strengthening and the volume fraction of Laves phase could include two phases, as shown by curve 1 in Fig. 4.2. At the first stage, when the mean size of Laves phase is fine enough and can provide effective strengthening, before the maximum point of curve 1, precipitation strengthening from Laves phase is definitely increasing with the volume fraction. At the second stage, when Laves phase grows into large size, precipitation strengthening effect from Laves phase begins to decline.

The interaction between the solution strengthening and the precipitation strengthening can be demonstrated by combining curves 1 and 2 into curve 3, which illustrates the entire strengthening effect change along with the volume fraction of Laves phase. At the beginning, the creep rupture strength can be enhanced by the formation of fine Laves phase particles, arrived at the peak of curve 3, and then it starts to drop due to the fast growth of Laves phase into large size. Thus, the two slope changes on the creep rupture strength versus rupture time curve are qualitatively interpreted.

4.2.3 *Effect of Stress on Microstructure Evolution*

Figure 4.3 shows the Vickers hardness versus creep rupture strength of the 10Cr steel and the three sites selected for Vickers hardness measurement. Site A is located near the fracture surface. Site B is within the homogenous deformation part in the gauge section and about 10 mm away from the fracture surface. Site C is at the head portion. The gauge section and head portion are two parts with different states. The former was under the creep state while the latter could be considered to be under a simple ageing state.

The hardness at sites A and B decreases with the rupture life. However, site C shows a much smaller and slower hardness decrease, compared with site A or B, in the time range from 437 to 8,354 h. It can be deduced that the applied stress in gauge section accelerates the decline of hardness.

The local brightness of a back-scattered electron (BSE) image in SEM is in direct proportion to the average atomic number of the atoms in that region. The atomic number of tungsten, molybdenum and chromium are 74, 42 and 24, respectively. As a result of containing a large amount of tungsten and molybdenum atoms, Laves phase should have higher brightness in back-scattered electron images, which makes it easy to distinguish Laves phase from the $M_{23}C_6$-type carbides and MX-type carbonitrides.

In addition to back-scattered electron image, TEM diffraction pattern and energy dispersive X-ray spectrometry (EDS) analysis can distinguish Laves phase from $M_{23}C_6$-type carbide. However, opposite to the BSE image, the local

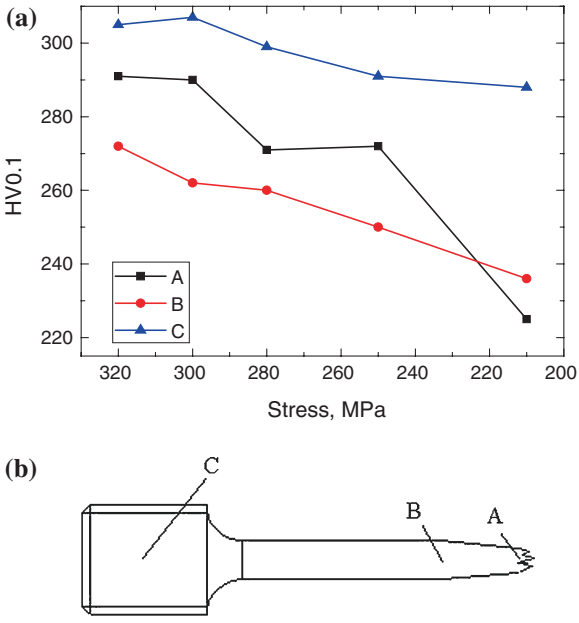

Fig. 4.3 Vickers hardness versus creep rupture strength of the 10Cr steel (**a**) and the sites for Vickers hardness measurement on the creep specimen (**b**). Reprinted from Hu et al. (2011), with permission from Elsevier

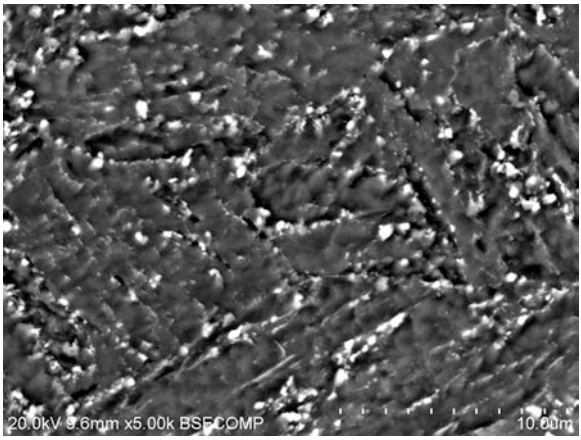

Fig. 4.4 SEM back-scattered electron micrograph of the 10Cr steel aged for 8,354 h. Reprinted from Hu et al. (2011) with permission from Elsevier

brightness of a TEM bright-field image is in inverse proportion to the atomic number of the atoms in that region, which gives Laves phase a darker appearance than $M_{23}C_6$-type carbide.

After creep for 8,354 h, the microstructure evolution at the head portion of specimen is slower than that at the gauge section (Figs. 4.4 and 4.5). Smaller amount of Laves phase forms in the ageing part than in the crept part. Moreover, the martensitic lath structure is retained and no transformation of lath into subgrains is found in the ageing part. Therefore, smaller hardness degradation happens at the head portion due to the slower microstructure evolution.

Sawada et al. (2001) found that, compared with the head portion, loading stress could accelerate the growth rate of MX carbonitrides in the gauge section of the specimen. They thought that the mobile dislocations could act as fast diffusion

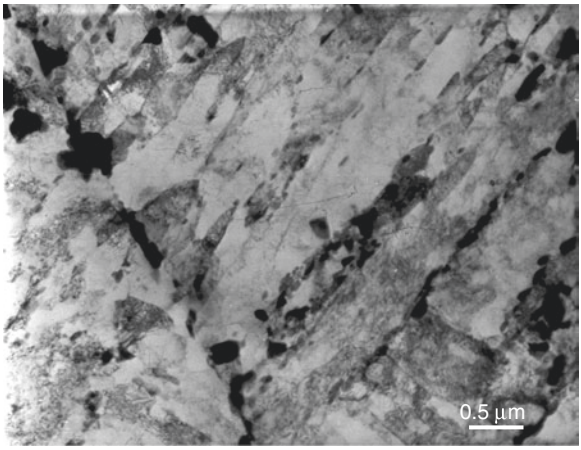

Fig. 4.5 TEM micrograph of the 10Cr steel aged for 8,354 h. Reprinted from Hu et al. (2011) with permission from Elsevier

pipes once they came across the MX carbonitrides. Fast diffusion of atoms led to the fast growth rate of these MX carbonitride precipitates. The applied stress can both increase the number of mobile dislocations and promote their movement, which will lead to two results:

(1) Due to the same pipe diffusion effect, Laves phase in the gauge section has large sizes and great amount;
(2) The laths would be much easier to transform into subgrains by dislocation migration.

In summary of Sects. 4.1 and 4.2, microstructure evolution takes place in 10Cr steel during creep, mainly exhibiting two aspects: (1) martensitic laths widening and evolving into subgrains, and (2) Laves phase growth and clustering along the prior austenite grain boundaries. The two slope changes on the creep rupture strength-life curve of the 10Cr steel are related to the precipitation behaviour of Laves phase. Stress accelerates the microstructure evolution.

4.3 Thermodynamic Calculations

The equilibrium state calculations show that no Laves phase should be found at 1,050 °C, the temperature for normalising. However, Laves phase should be present as an equilibrium phase at 760 °C, the temperature for tempering, and 600 °C, the temperature for creep. The equilibrium mass of Laves phase at 600 °C is around 1.6 %, larger than 0.6 % at 760 °C. It will take time for mass of Laves phase to reach the equilibrium. The volume percentage of Laves phase as a function of time at 760 °C and 600 °C is shown in Fig. 4.6. The Laves phase starts to form at 760 °C after a short incubation period of only 2,000 s, but its volume percentage can barely reach over 0.05 % even after tempering for 90 min. Therefore, it can be suggested that in the as tempered steel the dominant precipitates in the microstructure are MX and $M_{23}C_6$, and most of Laves phase in the steel should form during creep exposure at 600 °C. For the tempered steel under creep at 600 °C, Laves phase starts to precipitate after a long incubation period of almost 139 h, and then its volume percentage increases rapidly and reaches a plateau of about 1.6 % after nearly 8,334 h.

It is also illustrated in Fig. 4.6 that the formation of Laves phase can be clearly separated into two stages. One is the nucleation stage, which is characterised by the incubation period; the other is the growth stage, during which the volume percentage increases rapidly with time. When the growth of Laves phase is over, the coarsening stage begins. However, the volume percentage of Laves phase will keep constant in the coarsening period.

It is hinted by this calculation that Laves phase at the creep rupture are still at the growth stage since the longest rupture life is 8,354 h. Therefore, in the following, Laves phase will be discussed at the growth stage.

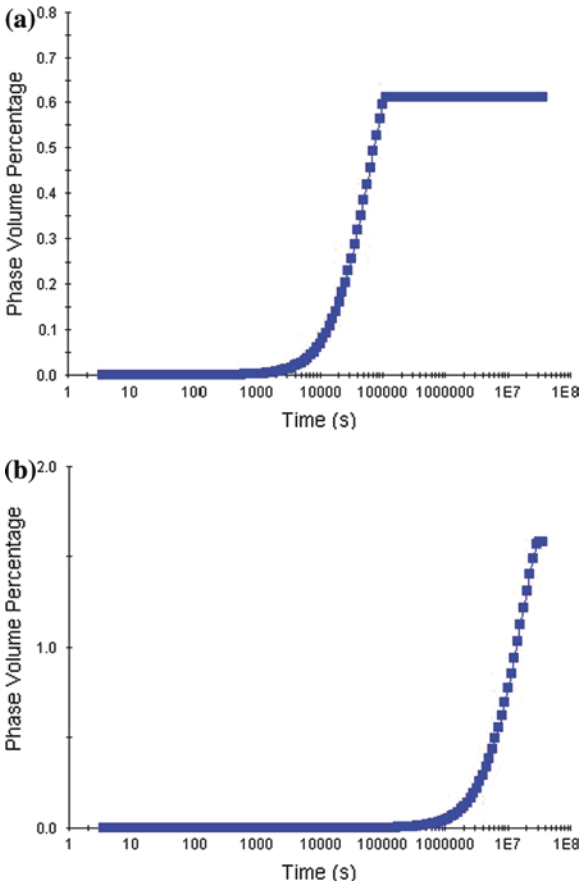

Fig. 4.6 Diagrams showing change of Laves phase volume percentage with time at (**a**) 760 °C and (**b**) 600 °C. With kind permission from Springer Science+Business Media: Frontiers of Materials Science in China, Hu et al. (2009)

4.4 Initial Microstructure and Growth of Laves Phase During Creep

Figure 4.7 is an optical micrograph of the initial microstructure of the tempered martensite. The prior austenite grain boundaries and lath boundaries are outlined by particles of $M_{23}C_6$ and MX precipitated during tempering. The δ-ferrite phase which often forms in the high Cr martensitic steels and is adverse to the creep rupture strength is scarcely found in this steel. The prior austenite grain size of the steel is about 15 μm.

Figure 4.8 shows the relationship between the applied stress and the rupture life in double logarithmic plot. In such a plot, the creep rupture strength linearly decreases as the rupture life extended. Experimentally, it was found that the amount of Laves phase increases with the endurance life from 430 to 3,230 h (Hu et al. 2009), consistent with the above prediction shown in Fig. 4.6b by thermodynamic calculations.

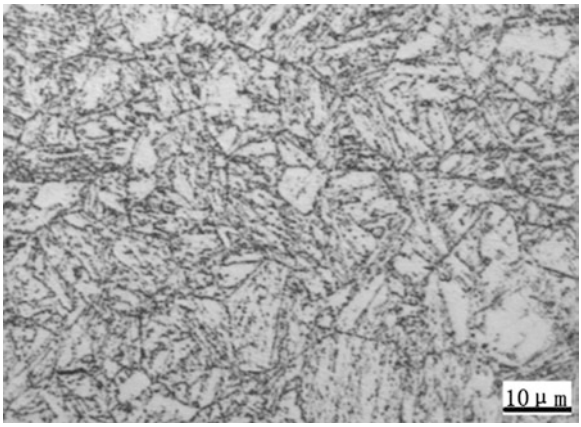

Fig. 4.7 Optical micrograph of the initial microstructure of the steel. With kind permission from Springer Science+Business Media: Frontiers of Materials Science in China, Hu et al. (2009)

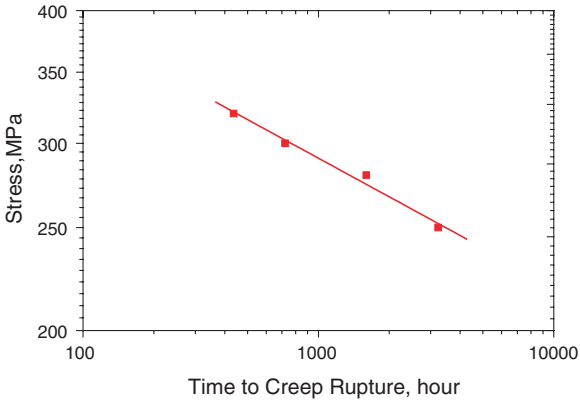

Fig. 4.8 The endurance curve of the steel in double logarithmic coordinates. With kind permission from Springer Science+Business Media: Frontiers of Materials Science in China, Hu et al. (2009)

Li (2006) pointed out that Laves phase would nucleate at martensite lath boundaries at first, keeping coherent with a lath, and then grow into the adjacent lath without a rational orientation. This morphology characteristic is helpful for identifying the Laves phase. In terms of morphology, there are three types of Laves phase: fine plate-shape and coarse rectangular shape Laves phase at lath boundaries, as well as coarse block-shape Laves phase in the matrix. According to Li (2006), the former two types of Laves phase should have a coherent orientation relationship with the adjacent lath. According to the growth process of Laves phase in the steel through the TEM observation with rupture life from 436 to 3,230 h (Hu et al. 2009), at the early stage of creep exposure, Laves phase prefers to distribute along lath boundaries. At the later stage of creep exposure, an increasing number of fully grown Laves phase distributes randomly inside the laths or subgrains. The mean size of Laves phase is more than 0.2 μm after 3,230 h which was much larger than that of $M_{23}C_6$, about 50 nm, under the same condition, which indicates that Laves phase is much easier to grow into large size than $M_{23}C_6$.

4.5 Effects of Size on Creep Behaviour and Cobalt

As part of their evolution process, the mean width of the martensitic laths increases with the endurance life during creep and the lath is evolved into the subgrain structure in some places after 3,230 h of creep exposure. Lath widening is caused by the migration of lath boundaries by absorbing free dislocations. On the one hand, reduction of the dissolved tungsten and molybdenum atoms due to the formation of Laves phase during creep would decrease the pinning effect and accelerate the migration of dislocations. On the other hand, the coherent Laves phases at laths boundaries could inhabit the migration of lath boundaries and retard the coarsening of laths. However, the fine coherent Laves phases would grow into incoherent ones, which would greatly decrease the effect of pinning dislocations and lath boundaries. Therefore, at the early stage of creep exposure, the loss of solid solution strengthening by reduction of tungsten and molybdenum in matrix could be compensated by the precipitation strengthening of the fine coherent Laves phase, whereas, at the later stage, large incoherent Laves phase would fail in this compensation. This change in the effect of Laves phase on creep strength of the steel agrees with the results on P92 obtained by Lee et al. (2006).

It was also found by Lee et al. (2006) that the Laves phase with average size beyond 0.13 μm could trigger the ductile-to-brittle fracture mode transition, the major cause of breakdown of creep rupture strength. However, in this steel discussed in this section, the mean size of Laves phase exceeds this threshold after only 1,598 h creep exposure (Hu et al. 2009). In addition, the steel ruptured at 3,230 h under stress of 250 MPa exhibits ductile fracture characterised by dimples, as shown in Fig. 4.9. The dimple morphology on the creep rupture surfaces suggests ductile transgranular fracture. Therefore, there must be reasons other than the large Laves phase that should be responsible for the fracture mode transition from ductile transgranular to brittle intergranular. The coarsened Laves phases are the favoured nucleation sites for creep cavities. On the short-term creep exposure,

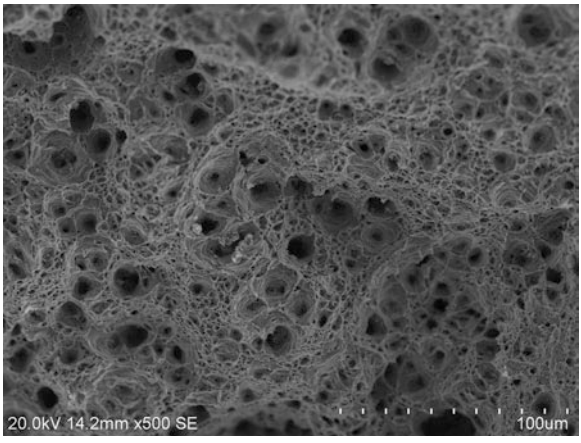

Fig. 4.9 Fracture surface of the steel ruptured at 3,230 h under 250 MPa. With kind permission from Springer Science+Business Media: Frontiers of Materials Science in China, Hu et al. (2009)

there are numbers of large Laves phase particles within grains. These large Laves phase precipitates within grains first generate a great number of creep cavities inside grains, which are then linked together through propagation of transgranular cracks before rupture, resulting in the ductile transgranular fracture. However, Laves phase would aggregate along the prior austenite gain boundaries during creep exposure, as shown in Fig. 4.10. If the mass of Laves phase in the microstructure is assumed to be constant after long-term creep exposure, the density of the coarsened Laves phase would increase along grain boundaries but decrease inside grains. The high density of the coarsened Laves phase along the prior austenite grain boundaries produced dense creep cavities along grain boundaries, which should be associated with the brittle intergranular fracture. In fact, Lee et al. (2006) observed that creep cavities were usually attached to large Laves phase precipitates on grain boundaries when brittle intergranular fracture took place, but they did not give an explanation why coarsened Laves phase particles on grain boundaries became the preferential nucleation sites for creep cavities.

The growth rate is controlled by diffusion. It is believed that cobalt can retard the diffusion of metal atoms in steels, because the diffusion coefficient is dependent on the Curie-temperature that is raised by cobalt addition. Various precipitation phenomena are retarded by cobalt. Therefore, the addition of cobalt is supposed to inhibit the growth of Laves phase. Hald (2008) found that the size of Laves phase reached nearly 0.1 μm after about 10,000 h creep exposure and almost stayed constant at 600 °C in P92 steel. Lee et al. (2006) also found that the size of Laves phase increased to nearly 0.13 μm after about 25,000 h creep-exposure at 600 °C in P92 steel. However, the average size of Laves phase has arrived at about 0.2 μm after only 1,598 h in the present new steel. The fact that Laves phase shows faster growth rate in this steel with cobalt addition than that in P92 steel without cobalt conflicts with those results that cobalt had an effect of retarding precipitation.

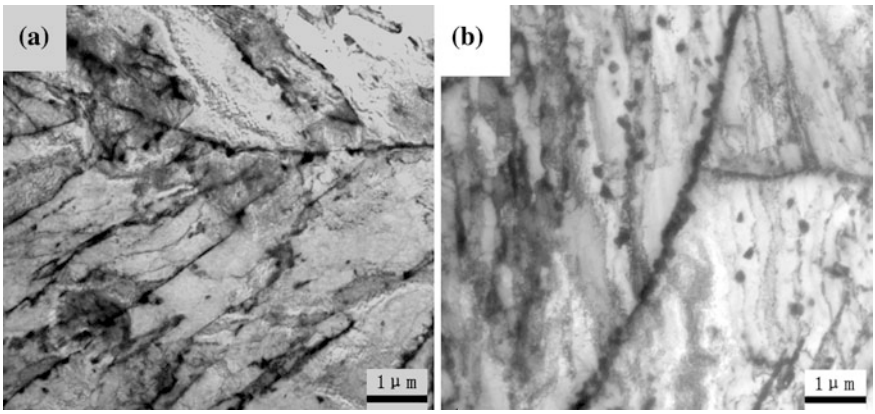

Fig. 4.10 TEM images showing the aggregation of Laves phase along prior austenite grain boundaries. **a** 436 h, 320 MPa; **b** 1,598 h, 280 MPa. With kind permission from Springer Science+Business Media: Frontiers of Materials Science in China, Hu et al. (2009)

Cobalt is also an important element added in maraging steels and there were also arguments on the influence of cobalt on their precipitate behaviour. Experiment on maraging steel suggests that cobalt could lower the solubility of molybdenum in matrix and promote the precipitation of Laves phase (Fe_2Mo). In the work on Fe-10 %Cr-6 %W alloys conducted by Cui et al. (2001), cobalt was found responsible for enhancement of growth of the Laves phase. Comparing the growth rate of Laves phase between P92 steel and the present new steel, it can be inferred that cobalt in this steel could accelerate rather than inhabit the growth of Laves phase, which may be explained by considering that cobalt can prevent the formation of δ-ferrite phase so that more tungsten and molybdenum can be kept in the matrix after normalisation, which could provide both more atoms needed for the growth of Laves phase and the driving force.

In summary of Sects. 4.3–4.5, in 10 % Cr heat-resistant steel containing cobalt, the Laves phase grows to a large size in a relatively short exposure time. With increase of the creep exposure time, Laves phase not only grows larger but also loses its coherent relationship with the adjacent lath, which could cause a loss of precipitation strengthening. In addition, the increasing number of Laves phase precipitates could decrease the solid solution strengthening effect due to the consumption of dissolved tungsten and molybdenum atoms. Decreases in both precipitation strengthening and solution strengthening effects should be the two reasons for degradation of creep rupture strength. The serious aggregation of large Laves phase precipitates along the prior austenite grain boundaries rather than the large size Laves phase precipitates should be considered responsible for the transition of ductile transgranular fracture to the brittle intergranular fracture. Addition of cobalt is believed to accelerate the growth rate of Laves phase.

4.6 Microstructural and Mechanical Properties of Short-Term Thermally Exposed Steels

The long-term creep rupture strength and microstructure stability of the 9/12Cr heat-resistant steels have been improved by an alloying and optimised heat-treatment procedure (Gustafson and Ågren 2001). The most recent improvements have been achieved by cobalt or tungsten alloying (Helis et al. 2009; Yamada et al. 2003). For example, it has been confirmed that cobalt is one of the important alloying elements to suppress the δ-ferrite formation during the high temperature normalising process in 9/12Cr heat-resistant steels. In contrast, it is also believed that addition of 2–3 % cobalt could drastically improve the short-term creep strength. Similarly, a lower creep rate and higher creep rupture strength in tungsten-containing heat-resistant steels can be attributed to the effects of both precipitation of Laves phase (Fe_2W) or μ phase (Fe_7W_6), as well as solid solution strengthening resulting from the addition of tungsten, which produces larger lattice misfit than molybdenum.

However, during thermal exposure, the steels containing cobalt or tungsten will undergo a microstructural change, leading to the degradation of their mechanical properties. It was found that the $M_{23}C_6$ and MX carbides coarsened, and Laves phase precipitated, during long-term exposure of a 12Cr steel containing tungsten (Kadoya et al. 2002). Most heat-resistant steels containing a high content of tungsten or cobalt show ductile-to-brittle transition with an increase of the rupture life, and it has been found that creep cavities are easily nucleated at coarse precipitates of Laves phase along grain boundaries. These findings suggest that, on the one hand, tungsten or cobalt can promote the precipitation during short-term thermal exposure, but, on the other hand, it can accelerate the coarsening of the precipitates during the long-term exposure process. When the coarsened Laves phase precipitates or carbides are greater than a critical size, the cavity formation is triggered and the consequent brittle intergranular fracture occurs (Lee et al. 2006; Abe 2004; Sawada et al. 2001). During the exposure process, the precipitated particles may crack or become detached from the matrix, and cavities may form in the microstructure. These might eventually affect the fracture mode of the ferritic steels during subsequent deformation, at ambient temperature.

Previous research has often focused on the mechanical properties and microstructure evolution of 9/12Cr heat-resistant steels after long-term exposure or under deformation creep. Few studies have discussed the change of microstructure under short-term thermal exposure. The study on microstructure evolution under short-term thermal exposure will play a complementary role in comprehensively understanding the effect of temperature and stress on the structural stability of 9/12Cr heat-resistant steels. In Sects. 4.7–4.10, based on the chemical composition of ASME-P92, through tungsten and cobalt additions, two ferritic/martensitic steels were designed and then fabricated at the laboratory scale. Room-temperature mechanical properties and microstructure evolution of the 9/12Cr heat-resistant steel during thermal exposure will be analysed. The aim of these sections is to identify the reason for the low impact toughness of the short-term thermally exposed 9/12Cr heat-resistant steels. The effect of tungsten and cobalt additions on microstructure evolution and fracture characteristics of 9/12Cr heat-resistant steels is also discussed.

4.7 Effect of Thermal Exposure on Mechanical Properties

The room-temperature mechanical properties of the thermally exposed (at 600 °C) steels (Table 4.1) are summarised in Fig. 4.11. Short-term thermal exposure at 600 °C has small influence on tensile properties, including yield stress (YS), ultimate tensile strength (UTS), elongation to fracture (A) and reduction in area (Z). The UTS of 10Cr steel increases after exposure at 600 °C for 500 h, and it tends to be stable with a subsequent increasing in exposure time. The UTS of P92 and 9Cr steels is lower than that of 10Cr steel before and after exposure. It is assumed that the difference in UTS for different steels should not be related to the

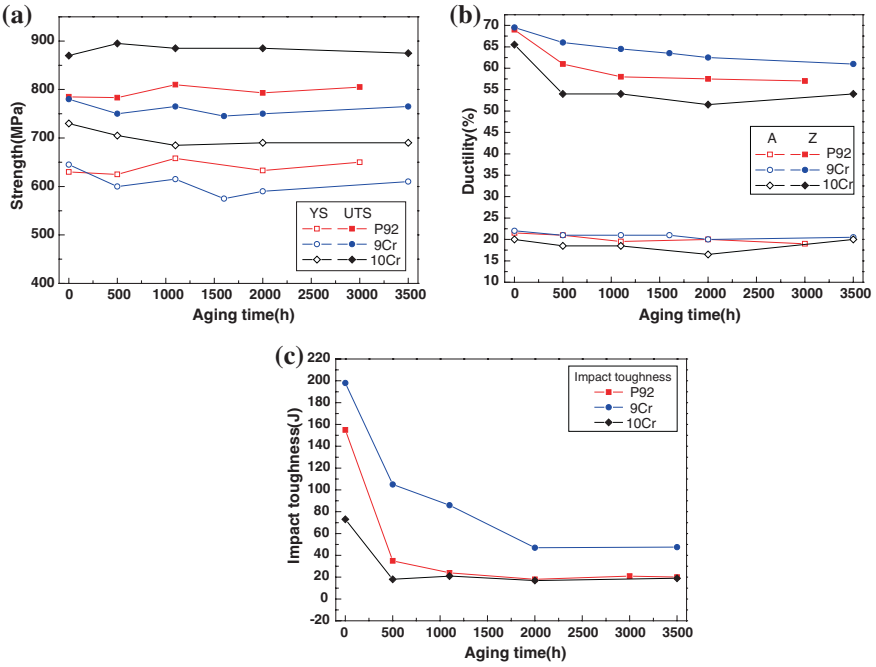

Fig. 4.11 Changes of (**a**, **b**) tensile and (**c**) impact properties with exposure time. Standard prismatic specimens ($10 \times 10 \times 55$ mm^3) with central V-shaped notch (2 mm in depth) were used for Charpy impact test. With kind permission from Springer Science+Business Media: Wang et al. (2012)

cobalt content but tungsten content. The reason for it can be analysed as follows. It is generally believed that 9/12Cr heat-resistant steels can be solution strengthened by additions of tungsten and cobalt, but for the current P92 and 9Cr steels, the addition of cobalt in 9Cr steel does not lead to increase of UTS. The 9Cr steel has 1.64 % cobalt, compared with the zero cobalt in the P92 (Table 4.1), but the UTS of the 9Cr steel is lower (Fig. 4.11a). If cobalt had a strengthening effect, then the 9Cr steel should have higher strength. Only when the content of tungsten is increased to 2.55 %, in 10Cr steel, is an increase approximately 100 MPa in UTS achieved.

Therefore, the effect of thermal exposure on tensile properties of the three steels is not significant. However, the influence of thermal ageing on the impact toughness is remarkable, as shown in Fig. 4.11c. The impact toughness of all three steels decreases dramatically when the exposure time is 500 h, and then the toughness tends to be stable with prolonged exposure time. Among the three steels, the 9Cr steel shows higher impact toughness than the other two steels. Thus, the impact data support the well known observation that most materials within a given microstructural class exhibit higher toughness with a decrease in strength (Chap. 7; Kim et al. 2008).

4.8 Effect of Thermal Exposure on Fracture Characteristics

Overall views on the impact fracture surfaces of the P92 steel after thermal exposure at 600 °C for different times are shown in Fig. 4.12. The fracture mode changes from ductile-to-brittle with increasing exposure time. The fracture mode of the tempered steel is characterised by transgranular ductile dimple tearing resulting from the coalescence of microvoids, but when the exposure time is 500 h, 100 % cleavage fracture is triggered. Especially, when the exposure time is extended to 3,000 h, an intergranular fracture characteristic is found near the cracking initiation site, as shown in Fig. 4.12c.

Figure 4.13 gives general views on the impact fracture surfaces of the 9Cr steel before and after thermal exposure. The 9Cr steel before thermal exposure shows the same fracture mechanism as the P92 steel. However, after thermally exposed for 500 h, the impact fracture surface is composed of both ductile zone and brittle zone. The area of the brittle zone increases with increasing exposure time. When the exposure time is 3,000 h, the entire fracture surface is brittle quasi-cleavage.

The fracture morphology of the 10Cr steel is different from the other two steels. Before thermal exposure, the fracture mode of 10Cr steel shows mixed rupture characteristics of brittle quasi-cleavage and dimples. After thermal exposure, it changes to completely brittle quasi-cleavage, as shown in Fig. 4.14.

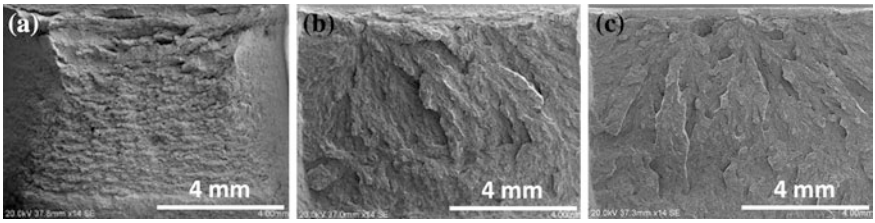

Fig. 4.12 SEM fractographs of impact specimens of the P92 steel after exposure for different periods of time. **a** 0 h; **b** 500 h; **c** 3,000 h. With kind permission from Springer Science+Business Media: Wang et al. (2012)

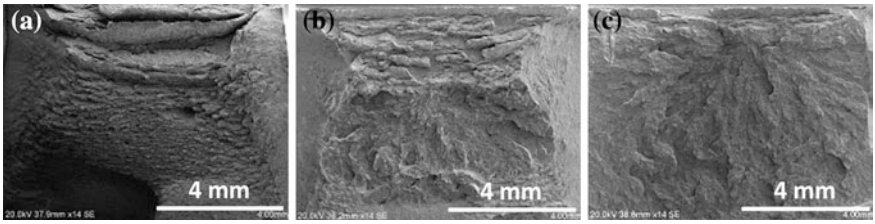

Fig. 4.13 SEM fractographs of impact specimens of the 9Cr steel after exposure for different periods of time. **a** 0 h; **b** 500 h; **c** 3,000 h. With kind permission from Springer Science+Business Media: Wang et al. (2012)

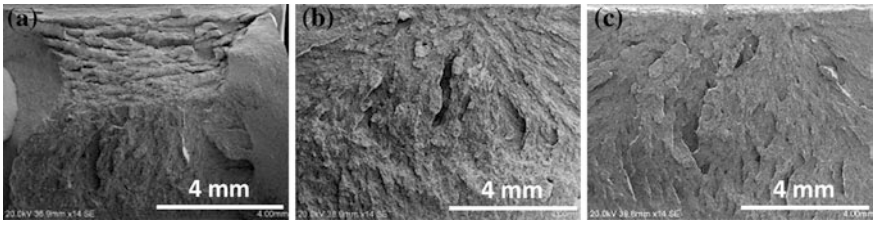

Fig. 4.14 SEM fractographs of impact specimens of the 10Cr steel after exposure for different periods of time. **a** 0 h; **b** 500 h; **c** 3,000 h. With kind permission from Springer Science+Business Media: Wang et al. (2012)

4.9 Effect of Thermal Exposure on Microstructure

During the thermal exposure, in contrast to tensile properties of the three steels, the impact toughness and the fracture mode exhibit considerable variations. Microstructural evolution under thermal exposure should be the main reason.

Figures 4.15a–c and 4.15d–f show SEM images of the three steels after thermal exposure for 500 and 3,000 h, respectively. Large amounts of fine precipitates distribute at the grain boundaries of prior austenite, martensite laths, and interior of the laths. The precipitates are carbide enriched with iron, chromium and tungsten. Also, nanosize MX-type carbonitrides form inside the martensite lath matrix. Helis et al. (2009), Kadoya et al. (2002), Lee et al. (2006), Abe (2004), Sawada et al. (2001) and Blach et al. (2009) found that additions of tungsten and cobalt could accelerate the growth of both carbide and MX carbonitride during thermal exposure, but these results came from the conditions of long-term exposure process or creep process. Here, the size of the carbide and MX carbonitride precipitates does not increase significantly during short-term thermal exposure process.

Ghassemi-Armaki et al. (2009) found that the coarsening rate of martensite lath was low during the exposure process. The three steels here also keep the structure of martensite as tempered after thermal exposure for 3,000 h, as shown in Fig. 4.16. These micrographs show little change in the martensitic structure of the tempered steels. The chemical compositions of the precipitates observed at the martensite interfaces are discussed subsequently in this section. Regarding the crystal structure of the precipitates, we will show a diffraction pattern of Laves-phase precipitates in Sect. 4.10. Their role on strengthening will also be discussed in Sect. 4.10. Without the effect of stress during the thermal exposure process, the carbide and MX could effectively retard the movement of dislocations at lath boundary or lath interior. Even after 3,000 h of thermal exposure, no obvious recovery could be triggered.

If no coarsening of carbide and MX happens and the recovery mechanism also is excluded, then what is the main reason for the difference of impact toughness after thermal exposure? In addition to carbide and MX, a change of another precipitate, Laves phase, should not be neglected (Kadoya et al. 2002;

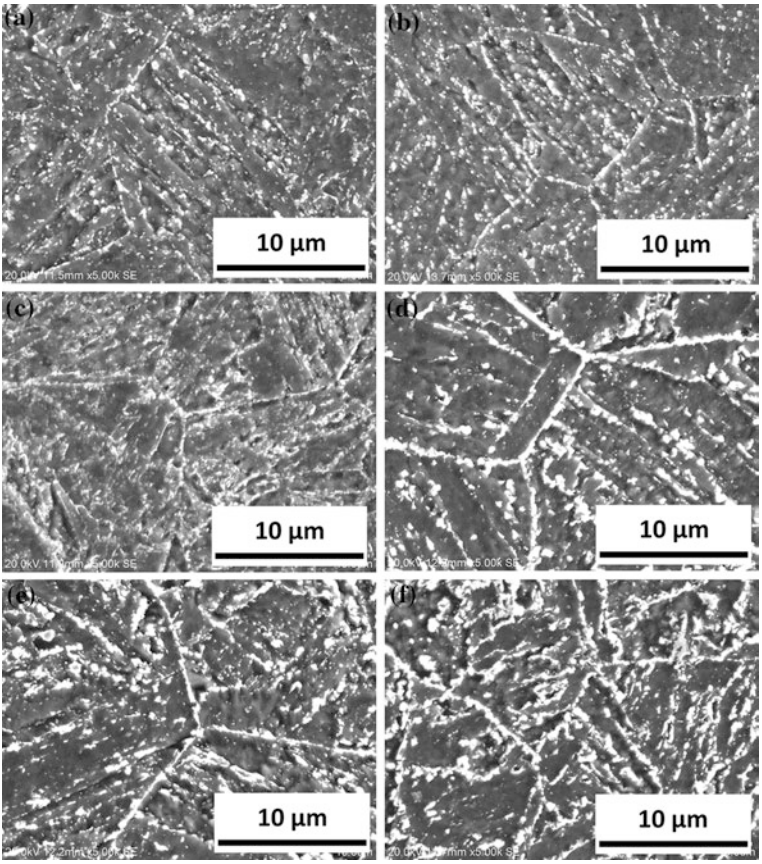

Fig. 4.15 SEM images of the microstructures after thermal exposure for 500 h and 3,000 h. **a** 500 h, P92 steel; **b** 500 h, 9Cr steel; **c** 500 h, 10Cr steel; **d** 3,000 h, P92 steel; **e** 3,000 h, 9Cr steel; **f** 3,000 h, 10Cr steel. With kind permission from Springer Science+Business Media: Wang et al. (2012)

Lee et al. 2006; Cui et al. 2001; Thomas Paul et al. 2008). Figure 4.17 shows the SEM BSE images of the three steels after thermal exposure for 500 and 3,000 h. As the brightness of SEM BSE image of a precipitate is determined by the average atomic weight of the compound, $M_{23}C_6$ type carbide should not be bright particles because its average atomic weight is lower than that of the matrix. In contrast, although ultrafine particles such as (V,Nb)(N,C) can be resolved in the SEM BSE images, the size of the precipitates does not increase significantly. As a result, Laves phase (Fe_2W) with bright contrast in Fig. 4.17 can be distinguished easily. The bigger particles with bright contrast in Fig. 4.17 contain tungsten element, which should be the Laves phase in the steels. With increasing exposure time, the number, volume fraction and size of Laves-phase precipitates increase.

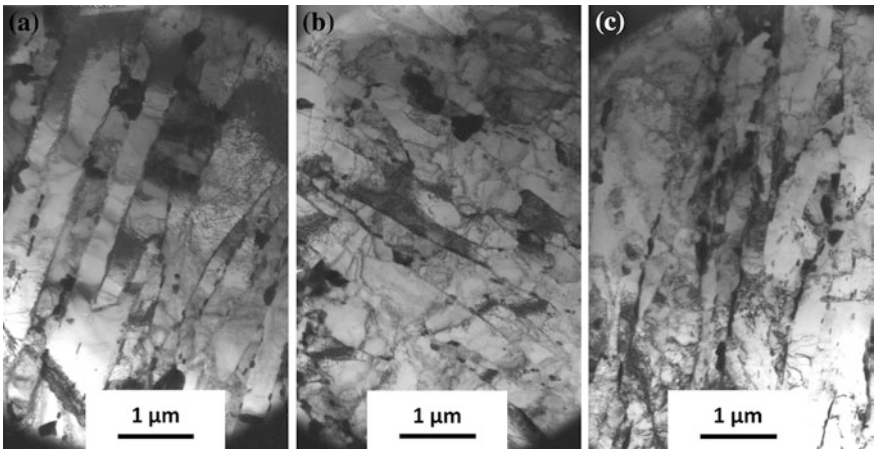

Fig. 4.16 TEM micrographs of martensitic lath structures after thermal exposure for 3,000 h, showing little change in the martensitic structure of the tempered steels. **a** P92 steel; **b** 9Cr steel; **c** 10Cr steel. With kind permission from Springer Science+Business Media: Wang et al. (2012)

Meanwhile, the EDS analysis in Fig. 4.18 show the different compositions of Laves-phase precipitates in P92 steel, 9Cr steel and 10Cr steel after 3,000 h thermal exposure. Microstructure characterisation in the form of the EDS spectra of the precipitates indicates the enrichment of tungsten in them. It should be noted that, in the EDS analysis in connection with an SEM, the spatial resolution is of the order of 1 μm. As these precipitates are much smaller than this size, the EDS data are not the actual precipitate compositions but are compositions of the precipitate and the surrounding matrix, with a total volume of the order of 1 μm^3. The precipitate under analysis will only be a small fraction of this volume, and the magnitude of this small fraction varies from one precipitate to another, depending on the exact size of the precipitate being measured. Therefore, the variation of the measurement results of different precipitates is dominantly controlled by this factor, and not the statistical factors. For this reason, the statistical errors would be much smaller than the errors caused by the inherent spatial resolution of SEM–EDS, when measuring composition of particles much small than this resolution. The contents of tungsten and likely molybdenum in Laves-phase precipitates in the three steels are underestimated, because of the contribution from the matrix surrounding the small precipitates. An increase of tungsten or cobalt content in steel can promote the precipitation of Laves phase, and accelerate the incorporation of tungsten in Laves phase. Other than the newly formed Laves phase the number and size of the original precipitates, i.e. carbide and MX in the three steels almost remain the same as in the tempered state, even after exposure for 3,000 h. Therefore, the remarkable decrease of impact toughness should be attributed to the precipitation and growth of Laves phase in the steels.

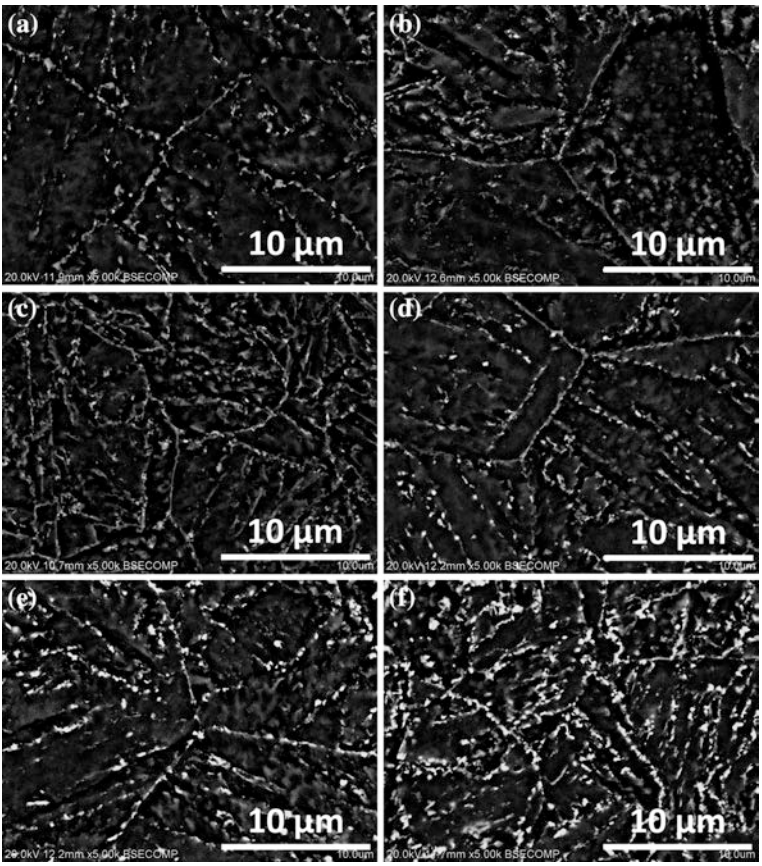

Fig. 4.17 SEM BSE images of the steels after thermal exposure for 500 h and 3000 h. The bright particles in the figures are Laves phase. **a** 500 h, P92 steel; **b** 500 h, 9Cr steel; **c** 500 h, 10Cr steel; **d** 3,000 h, P92 steel; **e** 3,000 h, 9Cr steel; **f** 3,000 h, 10Cr steel. With kind permission from Springer Science+Business Media: Wang et al. (2012)

4.10 Effect of Microstructure Evolution on Mechanical Properties

During short-term thermal exposure process, the effect of cobalt and tungsten on the size and distribution of carbide and MX could be neglected, and the difference of mechanical properties could be mainly caused by the precipitation of Laves phase in the steel. However, the evolution process of Laves phase precipitation is affected by cobalt and tungsten in the steels.

There were disagreements on the role of cobalt and tungsten in the microstructural evolution of 9/12Cr steels. With the addition of tungsten, the diffusion coefficient of the steel matrix would be decreased, the dislocations movement

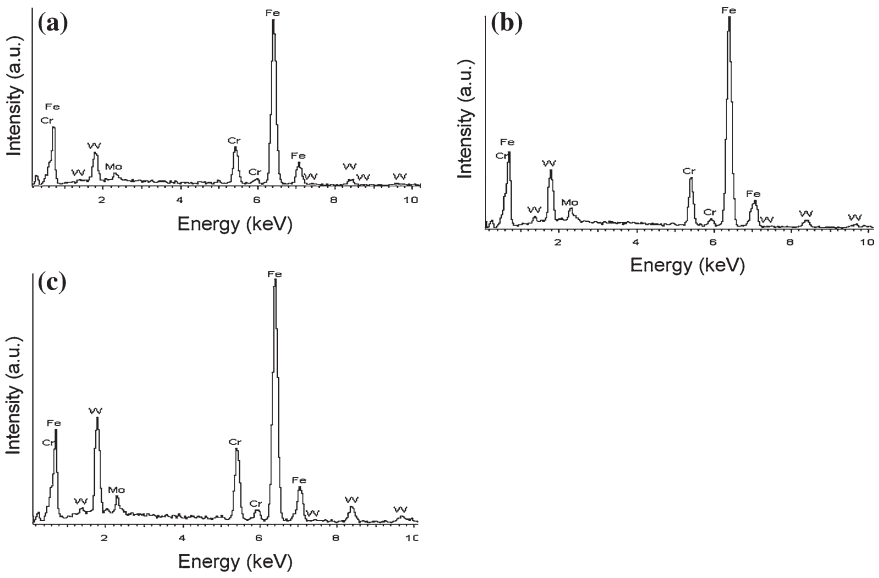

Fig. 4.18 SEM-EDS analysis of Laves phase in the microstructures after ageing for 3,000 h. **a** P92; **b** 9Cr; **c** 10Cr. With kind permission from Springer Science+Business Media: Wang et al. (2012)

and coarsening of carbide and recovery of martensite could be retarded, and eventually, the creep rupture strengths of the steels were increased (Abe 2004; Hasegawa et al. 2001). However, after long-term thermal exposure, the existence of tungsten would promote the formation and growth of Laves-phase precipitates in the steels, which would damage the impact property of the steels and the solution-strengthening effect of tungsten (Fernández et al. 2002). Especially when cobalt and tungsten are together added in 9/12Cr steels, the synergistic effect of the two elements on the microstructure and mechanical properties can be more remarkable. On the one hand, cobalt can retard the diffusion of metal atoms in steels because the diffusion coefficient of metal atoms is dependent on the Curie-temperature that is raised by cobalt addition. Therefore, the addition of cobalt can inhibit the coarsening of Laves-phase precipitates in the steels. On the other hand, the addition of cobalt can promote the precipitation of tungsten-containing compound from the steel matrix. It is well known that cobalt is an important element added in maraging steels because cobalt can decrease the solubility of molybdenum in the martensite matrix (He et al. 2002). Then, there should be more molybdenum taking part in the ageing reaction to strengthen the maraging steel, which is called the synergistic effect of cobalt and molybdenum in such type of steel. Regarding 9/12Cr steels, a synergistic effect of cobalt and tungsten is possible, as tungsten is similar to molybdenum in some ways.

As to the 10Cr steel with higher tungsten and cobalt contents, the driving force for the nucleation of Laves phase should be increased, and a large amount

of Laves phase could precipitate from the steel matrix. As shown in Fig. 4.17, the amount of Laves-phase precipitates in the 10Cr steel is much larger than that in 9Cr and P92 steels, for both times of exposure, 500 and 3,000 h. As a result, 10Cr steel has a higher tensile strength. However, why does 10Cr steel show lower impact toughness compared with the other two steels? It is believed that the incoherent Laves phase would trigger the fracture mode transition from ductile-to-brittle, as shown in Figs. 4.12, 4.13, 4.14. Lee et al. (2006) found that when the average size of Laves-phase precipitates exceeded 0.13 μm, the fine coherent Laves-phase precipitates would grow into the incoherent ones, which would greatly decrease their pinning effect on dislocations movement and lath boundaries. As shown in Fig. 4.17, with increasing exposure time and contents of tungsten and cobalt, more and more Laves-phase precipitates clustered along grain boundaries. Figure 4.19 shows the morphology of Laves phase precipitates in the 10Cr steel after exposure for 3,000 h, with size exceeding 0.1 μm. The large size and high density of Laves-phase precipitates along the grain boundaries would produce cavities at first and then lead to the brittle intergranular fracture.

It should be noted that Sects. 4.6–4.10 are not about creep strength, i.e. strength at the elevated temperature, but rather, they investigate the room-temperature strength and impact toughness after exposure at the elevated temperature. None of the discussions involve loading at the elevated temperature. Good ductility but poor impact toughness is an interesting phenomenon after the short-ageing process of these steels.

In summarising, Sects. 4.6–4.10 present the evolution of microstructure and mechanical properties of different 9/12Cr heat-resistant steels after short-term

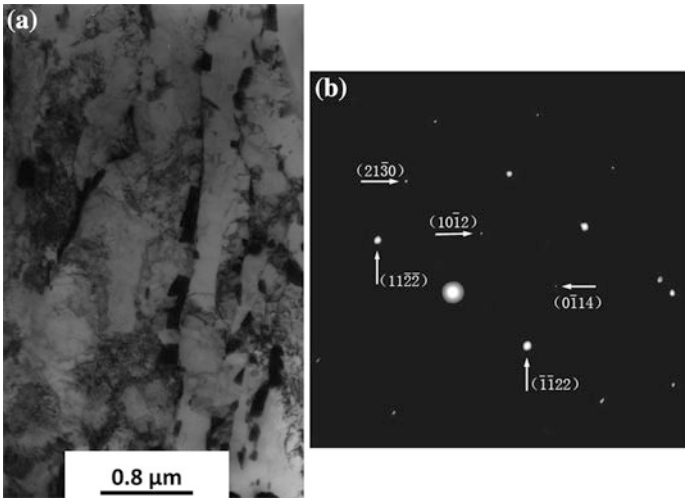

Fig. 4.19 Laves phase in the 10Cr steel thermally exposed for 3,000 h. **a** TEM bright-field image of coarse cubic Laves phase precipitates distributed at the lath boundaries, as well as coarse block Laves phase in the steel matrix; **b** diffraction pattern. With kind permission from Springer Science+Business Media: Wang et al. (2012)

thermal exposure. The tensile strength of 10Cr steel with higher cobalt and tungsten contents is higher than that of 9Cr with cobalt addition and commercial P92 steels, which have lower contents of cobalt and tungsten, but its impact toughness is lower than the other two steels. During short-term thermal exposure process up to 3,000 h, the effect of cobalt and tungsten on the size and distribution of carbide and MX can be neglected. The change of mechanical properties is mainly caused by the precipitation of Laves phase in the steels. On short-term thermal exposure, with increase of cobalt and tungsten contents, cobalt could promote the segregation of tungsten along the martensite lath to form Laves-phase precipitates. A large size and high density of Laves-phase precipitates along the grain boundaries could lead to the brittle intergranular fracture of the steels.

References

Abe F (2004) Coarsening behavior of lath and its effect on creep rates in tempered martensitic 9Cr–W steels. Mater Sci Eng A 387–389:565–569. doi:10.1016/j.msea.2004.01.057

Abe F, Semba H, Sakuraya T (2007) Effect of boron on microstructure and creep deformation behavior of tempered martensitic 9Cr steel. Mater Sci Forum 539–543:2982–2987. doi:10.4028/www.scientific.net/MSF.539-543.2982

Blach J, Falat L, Ševc P (2009) Fracture characteristics of thermally exposed 9Cr-1Mo steel after tensile and impact testing at room temperature. Eng Fail Anal 16:1397–1403. doi:10.1016/j.engfailanal.2008.09.003

Cui J, Kim IS, Kang CY, Miyahara K (2001) Creep stress effect on the precipitation behavior of Laves phase in Fe-10 % Cr-6 % W alloys. ISIJ Int 41:368–371. doi:10.2355/isijinternational.41.368

Fernández P, Hernández-Mayoral M, Lapeña J, Lancha AM, De Diego G (2002) Correlation between microstructure and mechanical properties of reduced activation modified F-82H ferritic martensitic steel. Mater Sci Technol 18:1353–1362. doi:10.1179/026708302225007411

Ghassemi-Armaki H, Chen RP, Maruyama K, Yoshizawa M, Igarashi M (2009) Static recovery of tempered lath martensite microstructures during long-term aging in 9–12 % Cr heat resistant steels. Mater Lett 63:2423–2425. doi:10.1016/j.matlet.2009.08.024

Gustafson Å, Ågren J (2001) Possible effect of Co on coarsening of $M_{23}C_6$ carbide and Orowan stress in a 9 % Cr steel. ISIJ Int 41:356–360. doi:10.2355/isijinternational.41.356

Hald J (2008) Microstructure and long-term creep properties of 9–12 % Cr steels. Int J Pres Ves Pip 85:30–37. doi:10.1016/j.ijpvp.2007.06.010

Hasegawa T, Abe YR, Tomita Y, Maruyama N, Sugiyama M (2001) Microstructural evolution during creep test in 9Cr–2W–V–Ta steels and 9Cr–1Mo–V–Nb steels. ISIJ Int 41:922–929. doi:10.2355/isijinternational.41.922

He Y, Yang K, Qu W, Kong F, Su G (2002) Strengthening and toughing of a 2800-MPa grade maraging steel. Mater Lett 56:763–769. doi:10.1016/S0167-577X(02)00610-9

Helis L, Toda Y, Hara T, Miyazaki H, Abe F (2009) Effect of cobalt on the microstructure of tempered martensitic 9Cr steel for ultra-supercritical power plants. Mater Sci Eng A 510–511:88–94. doi:10.1016/j.msea.2008.04.131

Hu P, Yan W, Sha W, Wang W, Guo Z, Shan Y, Yang K (2009) Study on laves phase in an advanced heat-resistant steel. Front Mater Sci Chin 3:434–441. doi:10.1007/s11706-009-0063-7

Hu P, Yan W, Sha W, Wang W, Shan Y, Yang K (2011) Microstructure evolution of a 10Cr heat-resistant steel during high temperature creep. J Mater Sci Technol 27:344–351. doi:10.1016/S1005-0302(11)60072-8

Kadoya Y, Dyson BF, McLean M (2002) Microstructural stability during creep of Mo- or W-bearing 12Cr steels. Metall Mater Trans A 33A:2549–2557. doi:10.1007/s11661-002-0375-z

Kim BC, Park SW, Lee DG (2008) Fracture toughness of the nano-particle reinforced epoxy composite. Compos Struct 86:69–77. doi:10.1016/j.compstruct.2008.03.005

Lee JS, Armaki HG, Maruyama K, Maruki T, Asahi H (2006) Causes of breakdown of creep strength in 9Cr-1.8W-0.5Mo-VNb steel. Mater Sci Eng A 428:270–275. doi:10.1016/j.msea.2006.05.010

Li Q (2006) Precipitation of Fe_2W laves phase and modeling of its direct influence on the strength of a 12Cr-2W steel. Metall Mater Trans A 37A:89–97. doi:10.1007/s11661-006-0155-2

Maruyama K, Sawada K, Koike J (2001) Strengthening mechanisms of creep resistant tempered martensitic steel. ISIJ Int 41:641–653. doi:10.2355/isijinternational.41.641

Sawada K, Kubo K, Abe F (2001) Creep behavior and stability of MX precipitates at high temperature in 9Cr-0.5Mo-1.8W-VNb steel. Mater Sci Eng A 319–321:784–787. doi:10.1016/S0921-5093(01)00973-X

Thomas Paul V, Saroja S, Vijayalakshmi M (2008) Microstructural stability of modified 9Cr-1Mo steel during long term exposures at elevated temperatures. J Nucl Mater 378:273–281. doi:10.1016/j.jnucmat.2008.06.033

Yamada K, Igarashi M, Muneki S, Abe F (2003) Effect of Co addition on microstructure in high Cr ferritic steels. ISIJ Int 43:1438–1443. doi:10.2355/isijinternational.43.1438

Wang W, Yan W, Sha W, Shan Y, Yang K (2012) Microstructural evolution and mechanical properties of short-term thermally exposed 9/12Cr heat-resistant steels. Metall Mater Trans A 43 A, pp 4113–4122. doi:10.1007/s11661-012-1240-3